EUROFUSION WPMST1-PR(16) 14744

M Bernert et al.

Power exhaust by SOL and pedestal radiation at ASDEX Upgrade and JET

Preprint of Paper to be submitted for publication in
22nd International Conference on Plasma Surface Interactions
in Controlled Fusion Devices (22nd PSI)

This work has been carried out within the framework of the EUROfusion Consortium and has received funding from the Euratom research and training programme 2014-2018 under grant agreement No 633053. The views and opinions expressed herein do not necessarily reflect those of the European Commission.

Power exhaust by SOL and pedestal radiation at ASDEX Upgrade and JET

M. Bernert[a,*], M. Wischmeier[a], A. Huber[b], F. Reimold[b], B. Lipschultz[d], C. Lowry[c], S. Brezinsek[b], R. Dux[a], T. Eich[a], A. Kallenbach[a], A. Lebschy[a], C. Maggi[e], R. McDermott[a], T. Pütterich[a], S. Wiesen[b], JET Contributors[f,1], the EUROfusion MST1 team[2], the ASDEX Upgrade Team

[a] *Max Planck Institute for Plasma Physics, Boltzmannstr. 2, 85748 Garching, Germany*
[b] *Forschungszentrum Jülich GmbH, Institut für Energie- und Klimaforschung - Plasmaphysik, 52425 Jülich, Germany*
[c] *European Commission, B-1049 Brussels, Belgium*
[d] *University of York, York Plasma Institute, Heslington, York, YO10 5DD, United Kingdom*
[e] *CCFE, Culham Science Centre, Abingdon OX14 3DB, UK*
[f] *EUROfusion Consortium, JET, Culham Science Centre, Abingdon, OX14 3DB, UK*

Abstract

Future fusion reactors require a safe, steady state divertor operation. A possible solution for the power exhaust challenge is the detached divertor operation in scenarios with high radiated power fractions. The radiation can be increased by seeding impurities, such as N for dominant scrape-off-layer radiation, Ne or Ar for SOL and pedestal radiation and Kr for dominant core radiation.

Recent experiments on the all-metal devices ASDEX Upgrade (AUG) and JET demonstrate operation with high radiated power fractions and a fully-detached divertor by N, Ne or Kr seeding with a conventional divertor in a vertical target geometry. For both devices similar observations can be made. In the scenarios with the highest radiated power fraction, the dominant radiation originates from the confined region, in the case of N and Ne seeding concentrated in a region close to the X-point.

Applying these seed impurities for highly radiative scenarios impacts local plasma parameters and alters the impurity transport in the pedestal region. Thus, plasma confinement and stability can be affected. A proper understanding of the effects by these impurities is required in order to predict the applicability of such scenarios for future devices.

*Corresponding author, *Email address: matthias.bernert@ipp.mpg.de*

[1] See the Appendix of F. Romanelli et al., Proceedings of the 25th IAEA Fusion Energy Conference 2014, Saint Petersburg, Russia

[2] See http://www.euro-fusionscipub.org/mst1.

1. Introduction

Future fusion reactors require plasma scenarios with high dissipated power fractions in order to reduce the power flux on the divertor target plates. For ITER, about 85-90% of the exhaust power needs to be dissipated and for a possible DEMO reactor a fraction of more than 95% is required to meet the material limits [1, 2]. With a sufficient reduction of the power flux to the divertor, the electron temperature in the divertor is reduced down to several eV, where atomic processes set in and volumetric recombination becomes efficient. In this detached state the particle and power flux to the targets reduces significantly.

The power dissipation consists of perpendicular transport, charge exchange losses and radiation losses, the latter usually being the biggest contribution. The radiated power can be increased by introducing seed impurities. These can be chosen to increase primarily the core (e.g. Kr, W) or scrape-off-layer radiation (e.g. N, Ne). In order to retain the enhanced energy confinement of the H-mode, the power flux across the separatrix has to stay above the L-H threshold [3]. Therefore, at ITER additional radiation in the core is not viable, while for DEMO the expected excess of alpha heating above the H-mode threshold allows (and requires) significant core radiation. [4]

High radiation scenarios with different seed impurities were tested at the two all-metal tokamaks ASDEX Upgrade (AUG) and JET. These experiments aimed to demonstrate power exhaust at highest heat fluxes. The dominant parameter determining these heat fluxes is the ratio of the power flux over the separatrix P_{sep} and the major radius of the plasma R [5]. For ITER, this is in the range of $P_{sep}/R \approx 15$ MW/m and for DEMO expected to be in the range of $15 - 20$ MW/m [1]. At AUG, values of up to $P_{sep}/R = 12$ MW/m were achieved, while at JET experiments were limited to about 5 MW/m.

This publication compares the observations at both machines and the impact of the various seed impurities on the plasma scenarios. It is ordered by the different seed impurities used, showing for both devices nitrogen seeding in section 2, neon seeding in section 3 and krypton seeding in section 4. Section 5 compares the observations at both devices and section 6 gives a summary and short outlook.

2. Nitrogen Seeding

The use of nitrogen for divertor cooling is a well established technique [6]. It is commonly observed that the energy confinement time of the plasma is increased with the injection of nitrogen in an all-metal device [7]. At the same time, the N seeding is observed to alter the ELM characteristics, increasing their frequency and decreasing the relative energy loss [8].

Figure 1a shows a tomographic reconstruction of the radiation distribution in AUG discharge #30506, where 18 MW of heating power are applied at a constant N seeding rate. The normalized confinement following the ITER physics base scaling [9] is around $H_{98} = 0.9$ at up to 95% of the Greenwald density. In between the type-III ELMs, the divertor is in a pronounced detached state [10], where the particle flux onto the target is significantly reduced for about 10 cm along the target. The radiated power fraction ($f_{rad} = P_{rad}/P_{heat}$) in this discharge is around 75%, while in discharges with lower heating power (e.g. AUG #29383) up to 90% of the heating power is radiated in the detached state.

In figure 1b a tomographic reconstruction of JET pulse 85067 is shown, where also 18 MW of heating power are applied. The plasma is in a ELM-free H-mode, the confinement is around $H_{98} = 0.7$ at 90% of the Greenwald density. The divertor is in a fully detached state and the radiated power fraction at about 75% (the maximum observed at JET [11]). At a higher heating power (JPN 87201, $P_{heat} = 27$ MW), the plasma is in a type-I ELMy H-mode but shows similar values of confinement and radiated power fraction as at 18 MW.

The comparison in figure 1 shows that for both devices, in N seeded detached discharges, the dominant radiation is emitted by a small region inside the confined region, above the X-point. In both cases, about 5 MW are radiated from this region, which is about 40% of the total radiation for JET and AUG.

For AUG, this so-called X-point radiator is consistently observed in the N seeded detached condition,

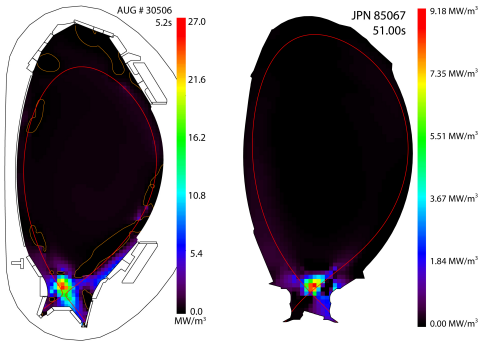

(a) AUG (b) JET

Figure 1: Radiation distribution of nitrogen seeded discharges at AUG (#30506) and JET (JPN 85067) in the detached state.

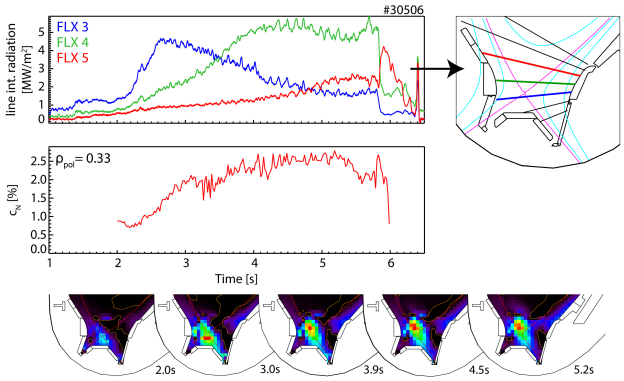

Figure 2: Evolution of radiation around X-point, line of sight measurements (top), central nitrogen concentration (middle) and temporal evolution of tomographic reconstruction (bottom).

not only at highest heating powers [12]. Such a local radiator inside the confined region can also be reproduced by modeling with the SOLPS code package [13].

Figure 2 shows the temporal evolution of the location of the X-point radiator in discharge AUG #30506, where a constant N seeding rate is applied. This constant seeding leads to a slow increase of the N concentration in the confined plasma due to the residence time of nitrogen in the vacuum chamber.The X-point radiator develops in the region of the X-point and with increasing N concentration moves upwards inside the confined region. It appears to be very localized and not significantly elongated along the magnetic field lines.

The intense radiation in this region indicates a strong reduction of the local temperature to values of $10 - 100$ eV, where N radiates efficiently. Electron temperatures of only a few eV are indicated by the SOLPS modeling and by the observation of deuterium line radiation in the region below the X-point radiator. However, there is no direct measurement of the electron temperature in this region available yet. Such a local reduction of the electron temperature might represent a so-called radiation condensation, where the characteristics of the impurity radiation lead to a strong cooling down to the temperature of the most efficient radiation. This leads to a density increase in this region and a further amplification of the radiation losses. This indicates a similarity of the X-point radiator to the MARFE phenomenon [14]. However, the operation with such a X-point radiator does not lead to an unstable plasma, as it is usually observed with MARFEs in tokamaks with carbon as first wall material. As shown in figure 2, this radiator can exist for several seconds and modulations by ELMs and heating power trips do not lead to an immediate end of the discharge.

Such strong poloidal asymmetries of radiation and electron temperature might be unexpected for the confined region of the plasma. However, the X-point region has a high flux expansion and, thus, inside the confined region, a long connection length to the midplane. Therefore, poloidal temperature gradients result in rather low parallel temperature gradients. This temperature gradient drives a power flux into the radiating region, which can be sustained by the radial power flux into the specific flux surface, and which stabilizes the temperature in this region. As the connection length is strongly changing at the X-point (if moving vertically upwards), the region of intense radiation might be determined by a local equilibrium between power flux driven into the region (determined by the parallel temperature gradient) and

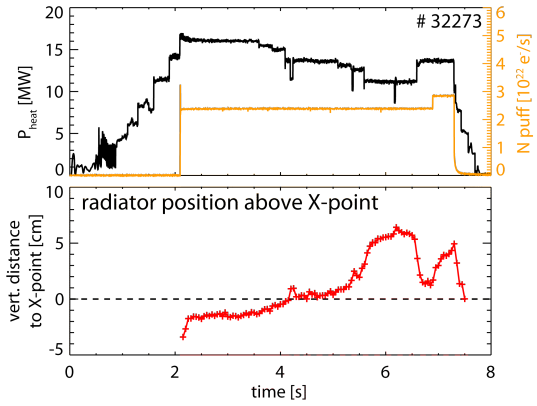

Figure 3: Vertical position of the radiator relative to the X-Point in AUG #32273 with the modulation of heating power and N seeding (top).

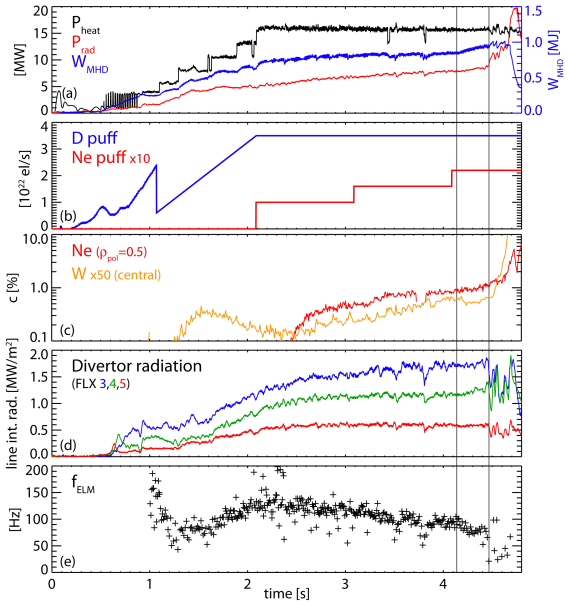

Figure 4: Time traces of Ne seeded discharge AUG #32272. The gray lines indicate when the confinement starts to increase and when the ELM frequency drops, respectively.

the radiated power. This can also be an explanation of the observed vertical movement of the X-point radiator.

Using the lines of sight of the AXUV diode bolometry [15], the vertical location and extend of the X-point radiator can be tracked. Figure 3 shows the vertical position relative to the X-point for discharge AUG #32273. By a reduction of heating power, this radiator moves further inside the confined region. With an increase of the heating power, the equilibration point of the radiator moves closer to the X-point. The increase of the N seeding levels leads again to an inward movement. If the radiator moves too far inside the confined region, a disruption is triggered (e.g. in AUG #32274).

The X-point radiator is observed in both devices, at AUG and JET, indicating that it is a general operational regime for devices with a full-metal wall. For both devices the radiator is, in detached conditions, inside the confined region and dissipating a significant fraction of the injected power by radiation. It still needs to be evaluated, in which way this radiation impacts the power flux over the separatrix, which determines the access to H-mode, and how the plasma confinement of such a scenario is affected.

3. Neon seeding

Neon is a promising candidate as an edge radiating impurity for future reactor scenarios. It radiates dominantly at temperatures of about 50 eV, which exist in the SOL. It does not trap tritium in the device as predicted for N, which potentially forms tritiated ammonia [16]. Therefore, high radiation scenarios with Ne instead of N seeding were tested at both devices, AUG and JET.

3.1. Ne seeding at AUG

Figure 4 shows time traces of a Ne seeded discharge #32272 at AUG. The Ne seeding level is increased in three steps. The first two levels lead to a slight increase of the central Ne concentration and the overall radiation level. However, the divertor radiation (Fig. 4(d)) is only marginally affected by the injected neon, showing that Ne does not increase the divertor radiation to required levels for efficient power exhaust (compared to N in Fig. 2). The presented discharge

is ended by a central accumulation of tungsten, which is caused by the Ne seeding.

The injection of Ne leads to an improvement of the confinement, here seen at 4.1 s, similar to the observations made with nitrogen. Unlike for N, where the pedestal top temperature is increased and, thus, leads to the confinement improvement [17], with Ne the pedestal top density is increased. Edge kinetic profiles before and after the confinement improvement are shown in figure 5(a).

The ratio of the neoclassical radial drift and diffusion coefficients for impurities, shown in figure 5(b), is calculated with the NEOART code [18]. The neoclassical inward drift, which dominates the pedestal impurity transport in between ELMs [19], increases significantly for Ne as well as for tungsten with the increased density gradient. This leads to an increase of the peaking factor of tungsten at the pedestal

$$F_W = \frac{n_W(\rho_{pol} = 0.97)}{n_W(\rho_{pol} = 1)} = \int_{1.0}^{0.97} \frac{v}{D} dr \quad [20]$$

from 5 to 35.

Furthermore, the ELM frequency is steadily reducing during the Ne seeding (Fig. 4(e)). This is the typical behaviour of type-I ELMs due to the reduction of the heating power [21]. In the present case, the central radiation of Ne reduces the actual power flux over the separatrix and thus leads to the reduction of ELM frequency. By the decrease in the ELM frequency, the effect of impurity flushing by ELMs [19] is significantly reduced.

Both effects together, namely the increased neoclassical inward transport and the reduced ELM flushing, lead to a strong, self-amplifying increase of the impurity concentration in the confined plasma and, thus, the collapse of the discharge.

The lack of efficient divertor cooling and the above mentioned effects of impurity transport make it impossible to study power exhaust with Ne seeding at the tested AUG parameters. In future devices the pedestal impurity transport is expected to be very different from current experiments due to the higher pedestal temperature gradients and lower density gradients. The temperature screening of impurities increases and the density gradient driven inward

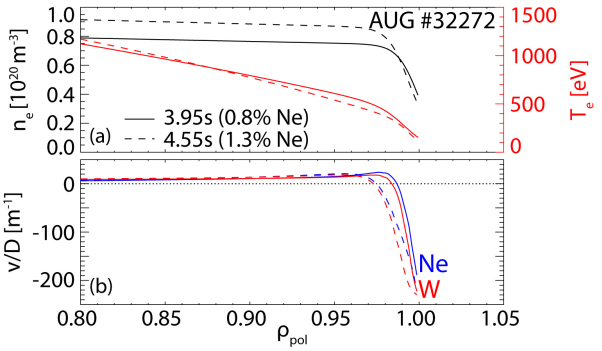

Figure 5: Top: Edge profiles of electron density and temperature before and after the confinement improvement. Bottom: NEOART calculation of the neoclassical impurity transport at the pedestal.

pinch reduces [22]. Therefore, the application of Ne seeding for power exhaust in such devices might still be possible.

3.2. Ne seeding at JET

At JET, Ne seeding to high radiated power fractions ($f_{rad} > 50\%$) leads to a dithering between ELM-free H-modes and L-modes and a confinement of $H_{98} \leq 0.8$ [11]. In these cases the dominant radiation is emitted from the region inside the X-point, similar to the observations with N seeding. With the dithering between H- and L-mode, the divertor goes from a detached (H-mode) to attached (L-mode) state. In H-mode the radiation is concentrated at the region just inside the X-point while in L-mode the radiation is more diffuse in the divertor and increased in the SOL (see Fig. 6).

The transitions between H- and L-mode indicate that the central radiation losses by Ne reduce the power flux over the separatrix below the L-H power threshold. In L-mode, the power flux over the separatrix is about 1 MW higher than in H-mode. This difference might determine the change between H- and L-mode, however, the power flux in H-mode is with 9.5 MW still above the L-H threshold scaling of about 8.7 MW.

The dithering between H- and L-mode makes Ne seeding also not applicable for power exhaust scenar-

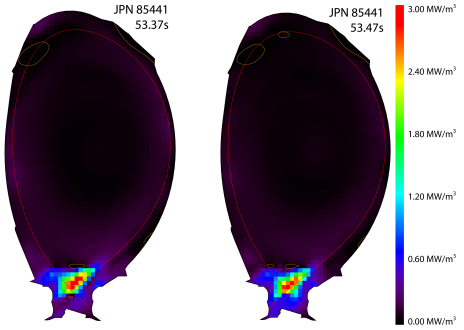

(a) H-mode, detached state (b) L-mode, attached state

Figure 6: Radiation distribution of the Ne seeded discharge JPN 85441.

ios at JET for the tested heating power of about 19 MW. With an external heating of more than 22 MW, the plasma might stay in H-mode and Ne could be further tested as a SOL and divertor radiator, however, such heating powers were not available for these experiments.

4. Krypton seeding

Krypton has a high radiation efficiency at electron temperatures of about 300 eV. Thus, it is expected to create strong radiation in the pedestal region inside the separatrix, as it is required for future fusion reactors. Additionally, at 15 eV the cooling factor of Kr has another peak, therefore, also increased radiation in a detached divertor can be expected.

4.1. Kr seeding at AUG

Figure 7 shows time traces of discharge AUG #33256, where Kr seeding is applied. Very low seeding rates of Kr are required ($\Gamma_{Kr} < 2e21\ el/s$), therefore, a gas puff modulation scheme is applied in order to achieve reliable particle fluxes from the gas valves. There is no effect seen by this modulation, indicating that the transport time scale of Kr is above 30 ms. In the presented discharge, a N puff was applied by a real time feedback [6] to keep the electron temperature at the outer divertor target around 5 eV. The

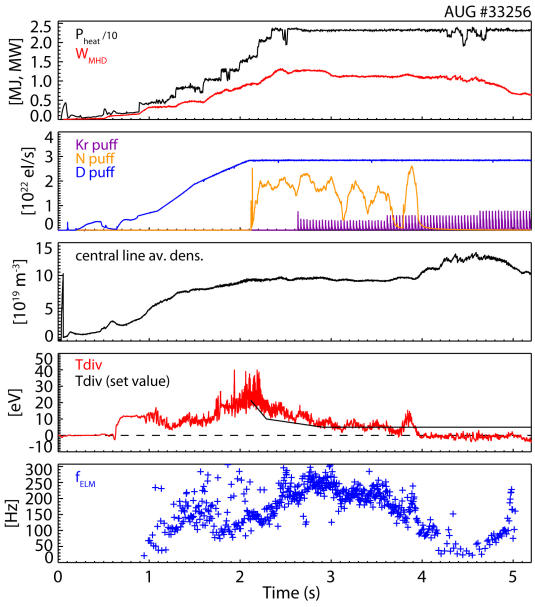

Figure 7: Time traces of Kr seeded discharge AUG #33256.

additionally injected Kr is stepwise replacing the N puff.

With the first step, there is only a small reduction on the averaged N seeding rate in order to keep the divertor temperature constant. The ELM frequency reduces slightly as the power flux over the separatrix is reduced by an increased central radiation. The drop in plasma stored energy at 3 s is caused by an internal 3/2 NTM, which develops at the high beta normalized of 2.7. This reduces the stored energy by 10%, which remains stable later on. Other plasma parameters do not change significantly.

With the second level of Kr seeding, the divertor goes into the detached state ($T_{div} \approx 0$ eV) and no further N seeding is required for divertor cooling. With Kr as dominant radiator, a radiating ring is forming around the pedestal region (see Fig. 8). The Kr radiation inside the confined region dissipates sufficient power to reduce the power fluxes onto the target plates to reach detachment. The radiated power fraction is up to 90%. This is observed with Kr concentrations of less than $5 \cdot 10^{-4}$ [23]. With the onset

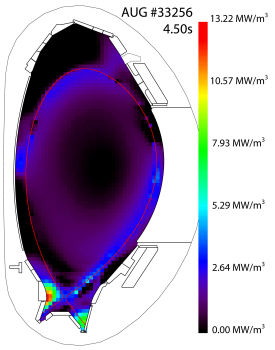

Figure 8: Radiation distribution (ELM averaged) with dominant Kr radiation for AUG #33256. The radiated power fraction is up to 90% and a radiating ring evolves at the pedestal. Such a radially narrow structure, which is most likely poloidally symmetric, cannot fully be reconstructed by the tomographic inversion (see Fig. 9 for details). The radiation in the divertor legs is dominated by ELM induced radiation.

of detachment, the plasma density increases by more than 30%.

Figure 9 shows the line integrated measurements of the pedestal radiation by AXUV diodes. The dominant radiation is emitted in the region of channel DHC44, which is dominantly measuring between $\rho_{pol} = 0.95 - 1$. This is identified by the strong signal increase from DHC43 to DHC44, but no further increase to DHC45. With the strong radiation inside the confined region, the ELM frequency reduces to

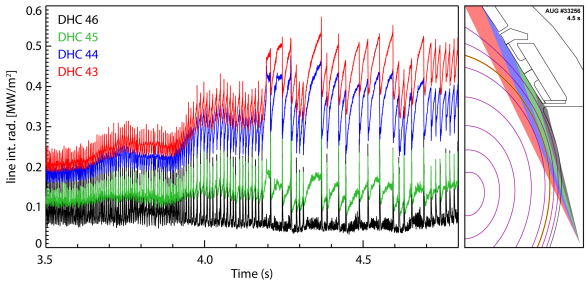

Figure 9: Left: Time traces of AXUV diode measurements at the pedestal region for AUG #33256. Right: Viewing volume of AXUV channels.

$10 - 20$ Hz.

In figure 9 the strong modulation of the pedestal radiation by ELMs can also be seen. In between ELMs, the pedestal radiation increases rapidly, while the pedestal is strongly eroded by an ELM. This can be explained by a strong inward transport of Kr in between ELMs, created by an increased density pedestal as shown in Sec. 3.1. Kr is cooling the pedestal region and, thus, leading to a further increase of the density. This is a self-amplifying process and leads transiently to hollow density profiles. The Kr in the pedestal region is flushed out by ELMs and the pedestal radiation is decreased. After an ELM, Kr is again transported inside.

At high ELM frequencies, the balance of inward transport and ELM flushing of Kr could potentially lead to a quasi steady state scenario. However, as Kr increases the central radiation and by this reduces the power flux over the separatrix, the ELM frequency is inherently reduced and the net inward transport of Kr is increasing. This results in a very low ELM frequency and a can lead to a (minor) radiative collapse of the plasma, seen in Fig. 7 at 4.8 s. Attempts to keep a high ELM frequency e.g. by additional N injection showed that the effect of Kr on the ELM frequency is still dominating. Therefore, other means of ELM frequency control are required and not yet tested.

The impact of the Kr radiation on the confinement depends on the radial location of the radiation. In discharges with high heating power ($P_{heat} =$ 19 MW), the pedestal top temperature is reduced by the Kr radiation from 1.2 keV to 800 eV. The region of maximum emissivity of Kr stays inside the pedestal region and the stored energy of the plasma is observed to not be affected. However, the subsequent effect on the ELM frequency and the resulting Kr influx leads to the collapse of the discharge.

In cases with lower heating power (e.g. AUG #31648, $P_{heat} = 10.5$ MW), Kr leads to a reduction of the pedestal top temperature from more than 500 eV to less than 400 eV. In these cases the dominant Kr radiation shifts further inside the confined region and the confinement is reduced by 20%. However, in these cases the ELM frequency remains high, mainly by a switching from type-I to type-III ELMs,

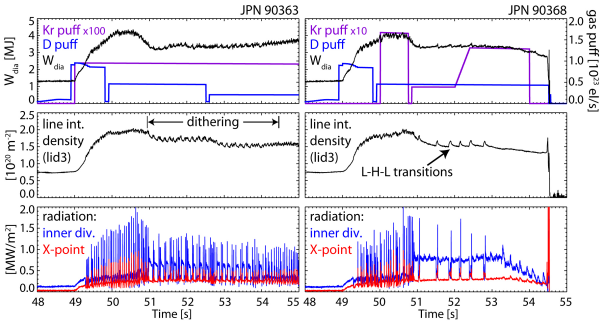

Figure 10: Time traces of JPN 90363 and JPN 90368, showing the dithering between H- and L-mode.

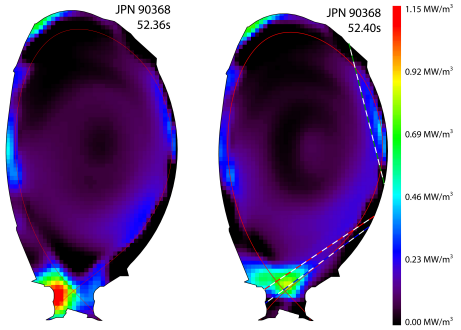

(a) L-mode, attached state (b) H-mode, detached state

Figure 11: Radiation distribution of the Kr seeded discharge JPN 90638. The radiation forms a poloidal ring in the pedestal region (which cannot be fully reconstructed). The dashed lines indicate the LOS of bolometry used in Fig. 10 & 12.

and the discharge continues at the low confinement level.

4.2. Kr seeding at JET

Experiments with Kr seeding at JET shows similar characteristics like at AUG. Figure 10 shows time traces of two Kr seeded discharges at a heating power of 18.5 MW. With the Kr seeding the confinement reduces and a dithering between L- and H-mode is observed. The H-mode phases are characterized by an increase in density and stored energy and the development of the temperature pedestal. In the L-mode phases density and stored energy decrease. The divertor switches from a detached outer target and radiation at the X-point in H-mode to an attached target and radiation in the inner divertor volume in L-mode. The maximum radiated power fraction is in the order of 65%.

In JPN 90368 the plasma stays in L-mode after 53.3 s. With the increased seeding, the divertor detaches and the pedestal radiation increases. This leads to a confinement reduction and finally to a disruption.

Figure 11 shows the radiation distribution of an H- and an L-mode phase in JPN 90368. The radiation inside the confined region is strongly increased and creates a radiating ring in the pedestal region, similar to the observations at AUG. However, at JET the radiation in the divertor and at the X-point appears to be more pronounced than at AUG. Nonetheless, the ratio of divertor to main chamber radiation (split at z=−1.1 m for JET and z=−0.66 m for AUG) is for both devices about 1:3.

The transport of Kr plays a major role for the observed dithering between H- and L-mode. This can been seen in the pedestal radiation, shown in figure 12. In the H-mode phase the pedestal radiation increases rapidly. At this phase the Kr is most likely transported inwards due to the neoclassical inward transport over the pedestal. In L-mode the gradients relax again and the neoclassical inward drift reduced. Turbulence is most likely dominating the Kr transport in these phases and the Kr is flushed out of the confined region. Therefore, the pedestal radiation reduces again.

This change of Kr transport and, thus, radiation characteristics of the plasma changes the power flux over the separatrix by about 2 MW (being higher in the L-mode). As the power flux is close to the L-H power threshold, such a change can determine whether the plasma is in L- or H-mode. The retarding effect of the Kr transport can then explain the dithering cycle of the Kr seeded discharges. Also the power flux into the divertor is altered by the two different regimes. With the reduced power flux of the H-

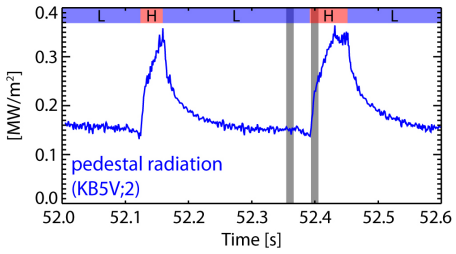

Figure 12: Line integrated measurement of the pedestal radiation by bolometry channel KB5V/2 in JPN 90368. The top bar indicates the L- or H-mode phase. The grey lines indicate the times of the tomographic reconstruction shown in Fig. 11.

mode, the divertor is detached between ELMs, while it is attached in L-mode.

The presence of the dithering between L- and H-mode does not depend on the amount of injected Kr. JPN 90363 and 90368 show for different seeding levels similar transitions and the impact on the confinement is comparable (see Fig. 10). However, the cycle time between H- and L-mode changes; at JPN 90368, the L-mode phases are up to 0.4 s long while in JPN 90363 they are shorter than 200 ms.

It might be possible to avoid the dithering by applying more heating power in order to stay significantly above the L-H power threshold. However, by the time of the execution of the experiments there was no additional heating power available and the data at higher heating powers is still pending.

5. Comparison between JET and AUG

Similar observations can be made for the high radiation scenarios at JET and AUG. With N seeding in both devices, strongly localized radiating regions inside the confined region above the X-point develop with the detachment of the divertor. For AUG, the confinement in these scenarios is only slightly reduced to $H_{98} \approx 0.9$, while at JET a stronger reduction to $H_{98} \approx 0.7$ is observed.

The scenarios compared at the two devices applied similar heating powers ($P_{heat} \approx 18 - 26$ MW), regardless of the machine size or L-H power threshold. Normalized to these values, the scenarios at JET have about a factor of two less heating power than at AUG. As observed by the dithering between L- and H-mode in Ne and Kr seeded scenarios at JET, the power flux over the separatrix is for these scenarios close to the LH power threshold. In comparison to the results from AUG, it can be expected that the confinement for the high radiation scenarios at JET is higher if more heating power (in the range of $30 - 35$ MW) would be applied.

6. Summary

High radiation scenarios with different seed impurities were tested at the two all-metal devices ASDEX Upgrade and JET. High dissipated power fractions and detached targets were achieved at both devices. These scenarios apply impurities which were expected to radiate inside the confined region (Kr) or in the SOL and divertor region (N, Ne). However, in detached divertor conditions, independent of seed impurities species, the dominant radiation is emitted from the confined region, mainly close to the X-point.

At AUG, the highest radiated power fraction for stable scenarios at high heat fluxes ($P_{heat}/R \leq 15$ MW/m^2) is in the order of 90%. The H-factor in these scenarios is between 0.75 and 0.9 while densities up to 95% of the Greenwald density are achieved. At JET, the highest achieved radiated power fraction is 75%. However, in both devices no significant power flux was detected in the divertor.

The experiments at both devices show that impurity seeding can have a strong effect on local plasma parameters. A radiation condensation at the X-point which might lead to poloidal asymmetric radiation and temperature profiles inside the confined region. Therefore, it is not sufficient to solely apply the temperature dependent cooling coefficient of an impurity on existing temperature and density distributions for the design of future high radiation scenarios.

Furthermore, the experiments show that impurity transport, especially in the pedestal region, is an important parameter for the stability of high radiation scenarios. This can be seen for both devices with Kr seeding and for AUG also with Ne seeding. Both impurities affect the pedestal parameters and the impu-

rity transport over the pedestal, which can lead to a self-amplification. Therefore, Ne and Kr seeding cannot be used for power exhaust studies at the tested AUG parameters, if no other means of impurity control, i.e. ELM pacing, are applied.

High radiation scenarios with detached targets are, nonetheless, a promising candidate to solve the challenge of power exhaust in future fusion reactors. The pedestal impurity transport is expected to be beneficial for such scenarios in these devices [22]. The application of Ar and of impurity mixes has to be tested further. The latter allows to tailor the radiation distribution in fusion plasmas and opens the possibility to optimize such scenarios for good confinement, stable scenarios and highest fusion gain.

Acknowledgment

This work has been carried out within the framework of the EUROfusion Consortium and has received funding from the Euratom research and training programme 2014-2018 under grant agreement No 633053. The views and opinions expressed herein do not necessarily reflect those of the European Commission.

References

[1] M. Wischmeier. High density operation for reactor-relevant power exhaust. *Journal of Nuclear Materials*, 463:22 – 29, 2015.

[2] A.S. Kukushkin, H.D. Pacher, G.W. Pacher, V. Kotov, R.A. Pitts, and D. Reiter. Consequences of a reduction of the upstream power SOL width in ITER. *Journal of Nuclear Materials*, 438, Supplement:S203 – S207, 2013.

[3] Y R Martin, T Takizuka, and the ITPA CDBM H-mode Threshold Database Working Group. Power requirement for accessing the H-mode in ITER. *Journal of Physics: Conference Series*, 123(1):012033, 2008.

[4] H. Zohm, C. Angioni, E. Fable, et al. On the physics guidelines for a tokamak DEMO. *Nuclear Fusion*, 53(7):073019, 2013.

[5] T. Eich, A.W. Leonard, R.A. Pitts, et al. Scaling of the tokamak near the scrape-off layer H-mode power width and implications for ITER. *Nuclear Fusion*, 53(9):093031, 2013.

[6] A Kallenbach, R Dux, J C Fuchs, et al. Divertor power load feedback with nitrogen seeding in ASDEX upgrade. *Plasma Physics and Controlled Fusion*, 52(5):055002, 2010.

[7] M N A Beurskens, J Schweinzer, C Angioni, et al. The effect of a metal wall on confinement in JET and ASDEX Upgrade. *Plasma Physics and Controlled Fusion*, 55(12):124043, 2013.

[8] P A Schneider, E Wolfrum, M G. Dunne, et al. Observation of different phases during an ELM crash with the help of nitrogen seeding. *Plasma Physics and Controlled Fusion*, 56(2):025011, 2014.

[9] ITER Physics Expert Group on Confinement, Transport, ITER Physics Expert Group on Confinement Modelling, Database, and ITER Physics Basis Editors. Chapter 2: Plasma confinement and transport. *Nuclear Fusion*, 39(12):2175, 1999.

[10] A. Kallenbach, M. Bernert, M. Beurskens, et al. Partial detachment of high power discharges in ASDEX Upgrade. *Nuclear Fusion*, 55(5):053026, 2015.

[11] A. Huber, M. Wischmeier, C.G. Lowry, et al. Impact of strong impurity seeding on the radiation losses in JET with ITER-like wall. *Europhysics Conference Abstracts (Proc. of the 41th EPS Conference on Controlled Fusion and Plasma Physics, Berlin, 2014)*, page P1.031, 2014.

[12] F. Reimold, M. Wischmeier, M. Bernert, et al. Divertor studies in nitrogen induced completely detached H-modes in full tungsten ASDEX Upgrade. *Nuclear Fusion*, 55(3):033004, 2015.

[13] F. Reimold, M. Wischmeier, M. Bernert, et al. Experimental studies and modeling of complete

H-mode divertor detachment in ASDEX Upgrade. *Journal of Nuclear Materials*, 463:128 – 134, 2015.

[14] B. Lipschultz, B. LaBombard, E.S. Marmar, et al. MARFE: an edge plasma phenomenon. *Nuclear Fusion*, 24(8):977, 1984.

[15] M. Bernert, T. Eich, A. Burckhart, et al. Application of AXUV diode detectors at ASDEX Upgrade. *Review of Scientific Instruments*, 85(3), 2014.

[16] M. Oberkofler, D. Alegre, F. Aumayr, et al. Plasma-wall interactions with nitrogen seeding in all-metal fusion devices: Formation of nitrides and ammonia. *Fusion Engineering and Design*, 98-99:1371 – 1374, 2015.

[17] A Kallenbach, M Bernert, R Dux, et al. Impurity seeding for tokamak power exhaust: from present devices via ITER to DEMO. *Plasma Physics and Controlled Fusion*, 55(12):124041, 2013.

[18] R. Dux and A.G. Peeters. Neoclassical impurity transport in the core of an ignited tokamak plasma. *Nuclear Fusion*, 40(10):1721, 2000.

[19] T. Pütterich, R. Dux, M.A. Janzer, and R.M. McDermott. ELM flushing and impurity transport in the H-mode edge barrier in ASDEX Upgrade. *Journal of Nuclear Materials*, 415(1, Supplement):S334 – S339, 2011. Proceedings of the 19th International Conference on Plasma-Surface Interactions in Controlled Fusion.

[20] T. Pütterich, R. Dux, E. Wolfrum, E. Viezzer, and the ASDEX Upgrade Team. Impurity transport within an ELM-cycle at the edge transport barrier in ASDEX Upgrade. *Europhysics Conference Abstracts (Proc. of the 36th EPS Conference on Controlled Fusion and Plasma Physics, Sofia, 2009)*, page P1.158, 2009.

[21] H Zohm. Edge localized modes (ELMs). *Plasma Physics and Controlled Fusion*, 38(2):105, 1996.

[22] Ralph M. Dux, Alberto Loarte, Clemente Angioni, David Coster, Emiliano Fable, and Arne Kallenbach. The interplay of controlling the power exhaust and the tungsten content in ITER. this conference, submitted to Nuclear Materials & Energy.

[23] M. Bernert, F. Reimold, R. Dux, et al. High radiation scenarios with radiation inside the confined region at ASDEX Upgrade. *Europhysics Conference Abstracts (Proc. of the 42nd EPS Conference on Controlled Fusion and Plasma Physics, Lisbon, 2015)*, page P1.135, 2015.